Volume 14
Number 22
14 June 2022
Pages 7947-8204

Nanoscale

rsc.li/nanoscale

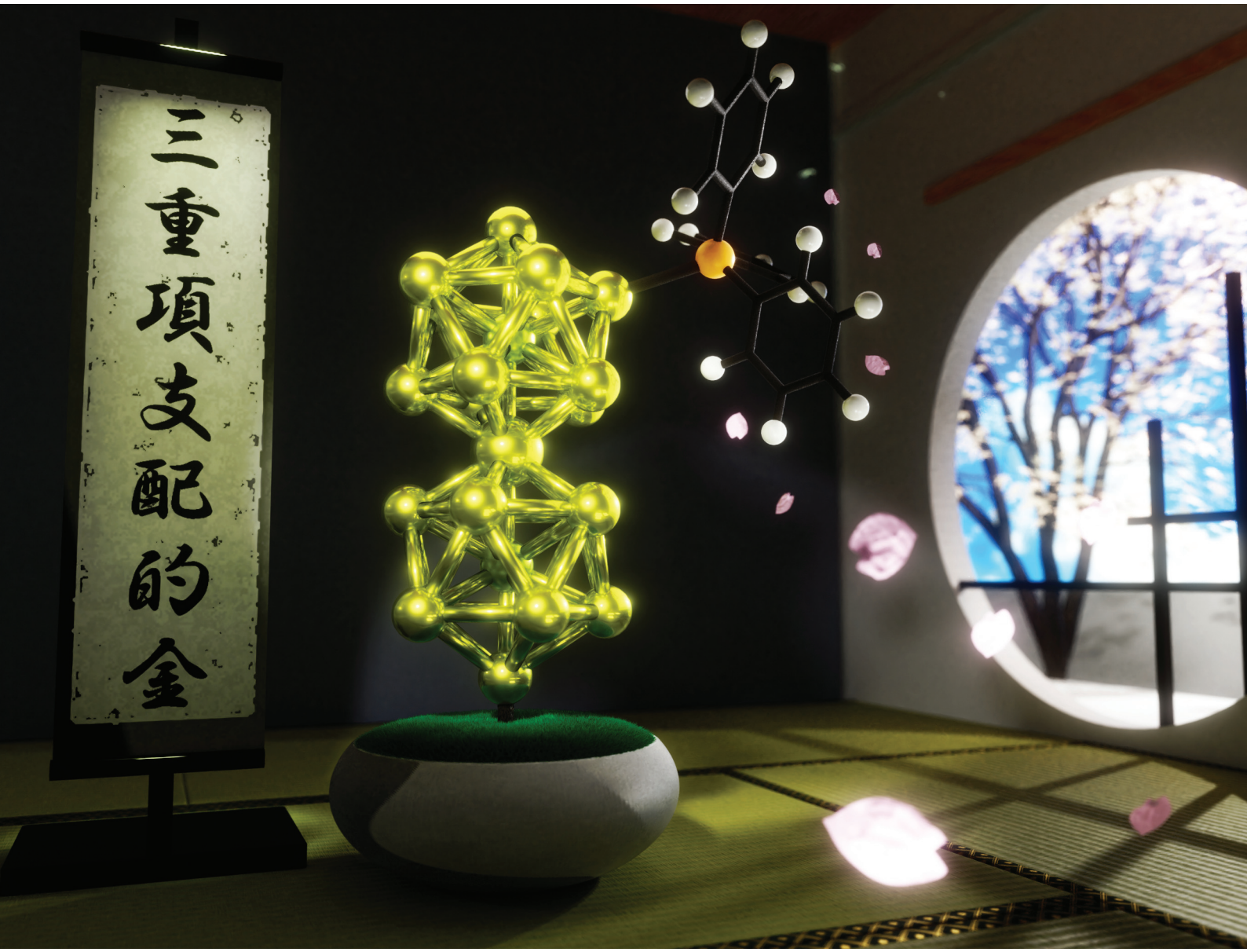

ISSN 2040-3372

ROYAL SOCIETY OF CHEMISTRY

COMMUNICATION
Masaaki Mitsui *et al.*
Evidence for triplet-state-dominated luminescence in biicosahedral superatomic molecular Au_{25} clusters

NCNST

Nanoscale

ROYAL SOCIETY OF CHEMISTRY

COMMUNICATION

View Article Online
View Journal | View Issue

Cite this: *Nanoscale*, 2022, **14**, 7974

Received 11th February 2022,
Accepted 5th April 2022

DOI: 10.1039/d2nr00813k

rsc.li/nanoscale

Evidence for triplet-state-dominated luminescence in biicosahedral superatomic molecular Au_{25} clusters†

Masaaki Mitsui, * Yuki Wada, Ryoto Kishii, Daichi Arima and Yoshiki Niihori

In photoluminescence (PL) quenching and triplet fusion upconversion experiments with fluorescent organic-molecule quenchers, it was revealed that a rod-shaped, phosphine- and thiolate-protected biicosahedral Au_{25} cluster (a representative di-superatomic molecule) exhibits only phosphorescence, not fluorescence, at room temperature with an intersystem crossing quantum yield of almost 100%. By virtue of these photophysical properties, this cluster can be used as a triplet sensitizer that undergoes direct singlet–triplet transitions in the near-infrared (NIR) region (730–900 nm), inducing photon upconversion from NIR to visible light.

Metal clusters of specific compositions and sizes often exhibit a peculiarly high stability and chemical robustness. As is well-known, these properties originate from geometrical and electronic factors.[1] The electronic factor is qualitatively explained by using the Jellium model,[2] which assumes that the valence electrons in a metal cluster are confined to a uniformly positive potential formed by constituent metal cations. This model predicts the existence of superatomic orbitals (1S, 1P, 1D, 2S...), discrete orbitals with similarities to atomic orbitals. Like noble gas atoms, clusters with closed-shell electron configurations of superatomic orbitals (the total number of valence electrons: 2, 8, 18...) are electronically stable. Therefore, metal clusters can be regarded as "superatoms" with electronic structures similar to those of normal atoms. The emerging creation of functional materials from superatom building blocks has recently gathered much attention.[3–7]

The most representative di-superatomic molecule is the rod-shaped, phosphine- and thiolate-protected gold cluster $[Au_{25}(PPh_3)_{10}(SR)_5Cl_2]^{2+}$ (henceforth abbreviated as Au_{25}-rod; PPh_3 = triphenylphosphine) formed by two icosahedral $Au_{13}{}^{5+}(8e^-)$ superatoms sharing a single vertex Au atom. As shown in Scheme 1, the Au_{25}-rod possesses an $Au_{25}{}^{9+}(16e^-)$ core. The crystal structure of this biicosahedral gold cluster was first reported by Tsukuda and co-workers.[8] Since then, the structural,[8–11] electronic,[8–12] catalytic,[13–15] photophysical,[16–19] and photoluminescence (PL)[18,20–22] properties of the Au_{25}-rod have been widely reported. The PL of the Au_{25}-rod has been dramatically enhanced by alloying with doping of Ag atoms.[23] Previous reports have suggested that the PL emission from the Au_{25}-rod is fluorescence.[18,23] However, this suggestion has not been backed by clear experimental evidence and requires further investigation. In addition, the PL quantum yield (Φ_{PL}) of the Au_{25}-rod was thought to be as small as 0.1%,[23] but the study reporting this conclusion was limited to the short-wavelength region (700–800 nm) of near-infrared (NIR) PL (700–1200 nm). More recently, the Φ_{PL} value was determined as ~8% over almost the entire NIR emission signal.[22] Motivated by these facts, we investigated the PL properties of the Au_{25}-rod cluster in more detail. In PL quenching and triplet fusion upconversion (TF-UC) experiments, we confirmed that the observed room-temperature PL of the Au_{25}-rod clusters actually originates from phosphorescence from the excited triplet state. The excited cluster exhibits no discernible fluorescence emission at room temperature and is exclusively deactivated by an intersystem crossing (ISC) process.

Fig. 1a shows the electrospray ionization mass spectrum of $[Au_{25}(PPh_3)_{10}(PET)_5Cl_2]^{2+}$ (PET = 2-phenylethanethiolate; counterion: SbF_6^-) synthesized in this study. The synthesis method was based on a previously reported method for the preparation of ultra-pure Au_{25}-rod samples (see the ESI† for details).[12] The strong signal at m/z = 4151.5 well matched the expected mass

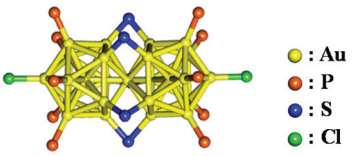

Scheme 1 Crystal structure of $[Au_{25}(PPh_3)_{10}(SR)_5Cl_2]^{2+}$.[8]

Department of Chemistry, College of Science, Rikkyo University, 3-34-1, Nishiikebukuro, Toshima-ku, Tokyo 171-8501, Japan. E-mail: mitsui@rikkyo.ac.jp

†Electronic supplementary information (ESI) available. See DOI: https://doi.org/10.1039/d2nr00813k

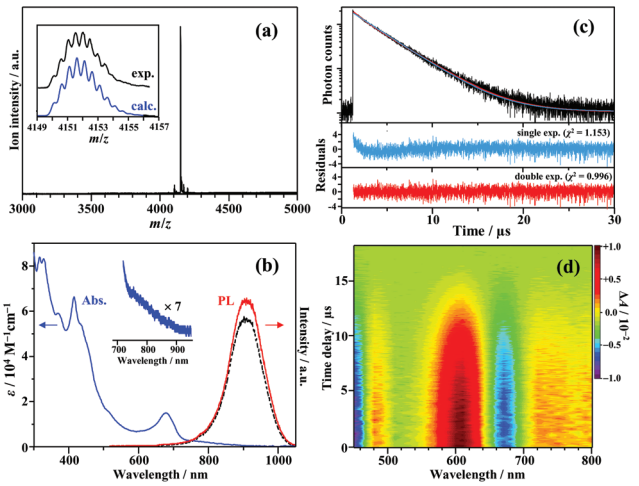

Fig. 1 (a) Positive-ion electrospray ionization mass spectrum of $[Au_{25}(PPh_3)_{10}(PET)_5Cl_2]^{2+}$ (Au_{25}-rod). (b) UV-vis absorption and PL spectra (λ_{ex} = 640 nm) of the Au_{25}-rod (13 μM) measured under deaerated conditions (the solid line) and aerated conditions (the dashed line). A magnified view of the absorption tail is also shown. (c) PL decay curve of the Au_{25}-rod (13 μM) in deaerated THF (λ_{ex} = 634 nm), obtained by monitoring the $\lambda \geq 750$ nm region, along with the single (red) and double (blue) exponential fitting curves. Bottom panels show the corresponding residuals and χ^2 values. (d) Color plot of the transient absorption spectra of the Au_{25}-rod (50 μM) in deaerated THF (pumped at 640 nm).

number when the charge number (z) was +2 (m/z 4151.6). The result confirms that the Au_{25}-rods were the dominantly formed product. The absorption and PL spectra of this sample are shown in Fig. 1b. The absorption spectrum with a weak absorption tail from 730 to 900 nm excellently agrees with the literature.[12,22] However, the peak around 900 nm in the PL spectrum is an artefact caused by a sharp drop in the sensitivity of the detector in this wavelength range (Fig. S1†), and the PL actually peaks at ~990 nm.[22] This NIR PL is observed in the wavelength region much longer than the lowest absorption band around 670 nm and is moderately weakened under aerated conditions, regardless of the excitation wavelength (Fig. 1b and Fig. S2†). The PL decay curve (depicted in Fig. 1c) was fitted to single and double exponential functions. The double exponential fit better reproduced the observed profile than the single exponential fit (see the residuals and χ^2 values in the lower part of Fig. 1c). Two lifetime components were identified, τ_I = 0.80 μs (3%) and τ_{II} = 3.36 μs (97%), with the average lifetime of 3.29 μs. Under aerated conditions, the PL lifetime and PL intensity were reduced by 10–20% compared to those under deaerated conditions (Fig. 1b, Fig. S2 and Table S1†), suggesting the involvement of oxygen in the PL quenching and the observed PL is assumed to stem from phosphorescence. The trace component (τ_I) was observed in the same wavelength range as the major component, and the PL lifetime was shortened and the fractional population slightly increased by the addition of a large excess of SbF_6^- (Table S2†), suggesting that the ion pairs of the Au_{25}-rod and SbF_6^- might be formed at a very low ratio by association–dissociation equilibrium in solution.[24,25] The lifetime of the dominant component excellently agrees with the reported average lifetime of the Au_{25}-rod (~3.2 μs).[22] Therefore, only the main component (τ_{II}) will be discussed below. Fig. 1d shows the sub-nanosecond transient absorption (TA) spectra of the Au_{25}-rod in deaerated THF. As reported in the literature, the overall feature of the TA spectrum (*i.e.*, excited-state absorption bands at around 480, 610, and >700 nm and ground-state breaching at 650–700 nm) was unchanged at all time delays.[16] These excited-state absorption bands are attributed to the T–T absorption of the Au_{25}-rod, as described later.

To experimentally confirm that the PL of the Au_{25}-rod is phosphorescence, PL quenching experiments were implemented on the Au_{25}-rod exposed to two highly fluorescent organic molecules, 9,10-bis(phenylethynyl)anthracene (BPEA) and rubrene, as the quenchers. When the Au_{25}-rod is combined with the BPEA or rubrene quencher, the expected main quenching pathway is triplet energy transfer (TET) (Fig. 2a and S3†). Indeed, both quenchers decreased the PL intensity and lifetime (Fig. 2b and c), but did not change the spectral shape of the Au_{25}-rod PL. Furthermore, there was no change in the absorption spectrum of the Au_{25}-rod up to the quencher concentration of 10 mM and no isosbestic point (Fig. S4†), thus ruling out the formation of association complexes between the Au_{25}-rod and BPEA (or rubrene). In the BPEA case, the Stern–Volmer plot of τ_{II} was a linear function of BPEA concentration up to 5 mM, but somewhat saturated at higher BPEA concentrations (Fig. 2d). As can be seen from the absorption spectrum in Fig. S4a,† BPEA aggregates begin to form when the BPEA concentration exceeds ~5 mM. Thus, the decrease in the effective quencher concentration due to the aggregation is considered to be the main cause of the downward deviation in Fig. 2d. In the presence of rubrene, the quenching effect was much more pronounced (Fig. 2c) and the linearity of the plot was maintained up to 10 mM (Fig. 2e). This result can be explained by the increased TET driving force due to the approximately 0.4 eV lower T_1 energy of rubrene [E_T = 1.14 eV] than that of BPEA [E_T = 1.53 eV] (Fig. 2a)[26] and the lack of rubrene aggregation in THF (Fig. S4b†). The linear dependence in the Stern–Volmer plot is a typical signature of dynamic quenching,[27] indicating that this quenching is solely based on collisions *via* diffusion. The Stern–Volmer constants (K_{sv}) obtained from the linear fits were 15.5 M^{-1} for BPEA and 320.1 M^{-1} for rubrene. From the relation $K_{sv} = k_{TET} \cdot \tau_{II}$, the TET rate constants (k_{TET}) in the presence of BPEA and rubrene were calculated as 4.6×10^6 M^{-1} s^{-1} and 9.5×10^7 M^{-1} s^{-1}, respectively. When anthracene [E_T = 1.84 eV][28] was used as the quencher, no quenching was observed at an anthracene concentration of 10 mM (Fig. S5 and Table S3†). Thus, we inferred that the T_1 state of the Au_{25}-rod is located around 1.6–1.7 eV. The magnitude of k_{TET} is obviously correlated with the energy gap between the T_1 states of the Au_{25}-rod and the quenchers (roughly +0.5 eV for rubrene, +0.1 eV for BPEA, and −0.2 eV for anthracene), indicating that the observed quenching is indeed caused by the TET process. Interestingly, even though the Au_{25} biicosahedral core is almost completely shielded by phosphine

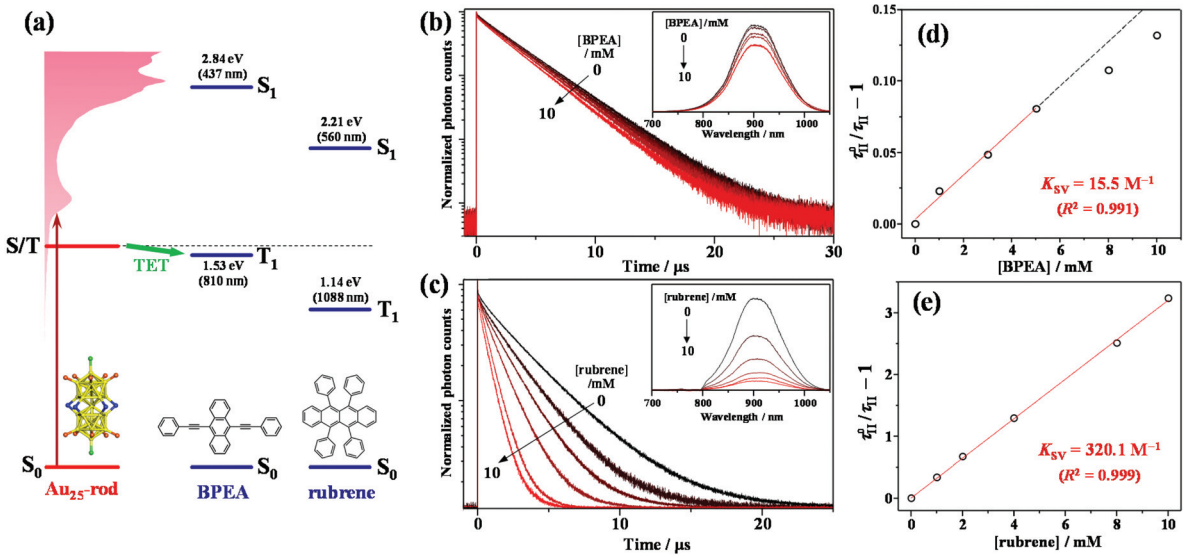

Fig. 2 (a) Energy-level diagram of the Au_{25}-rod sensitizer combined with a BPEA or rubrene emitter. (b and c) Emitter-concentration-dependent PL decay curves of the Au_{25}-rod (7 μM) in deaerated THF solution (excitation wavelength λ_{ex} = 634 nm). Insets in panels (b) and (c) show the corresponding PL spectra obtained under excitation with 640 and 785 nm CW lasers, respectively. (d and e) Stern–Volmer plots of the main component lifetime (τ_{II}). K_{SV} and R^2 represent the Stern–Volmer constant and coefficient of determination, respectively.

and thiolate ligands in the Au_{25}-rod (Fig. S6†), k_{TET} of the Au_{25}-rod for the rubrene acceptor is comparable to that of the $PtAg_{24}$ clusters (~10^8 M^{-1} s^{-1}), where the triplet excitation energy is transferred to the surface staple.[29] Notably, the Cl atoms bound to both ends of the long axis of the biicosahedral core are not completely shielded by the PPh_3 ligands. Moreover, in both the highest occupied molecular orbital (HOMO) and lowest unoccupied molecular orbital (LUMO), the p orbital of the Cl atom extends outward along the long axis direction of the Au_{25} core.[30] Therefore, these are presumed to be the effective sites for short-range Dexter-type TET to occur.

We attempted to measure the triplet–triplet (T–T) absorption of ^{3}BPEA* and ^{3}rubrene* sensitized by the TET from the Au_{25}-rod. However, the T–T absorption band overlapped with its own extremely strong S_0–S_1 absorption and could not be observed. If triplet sensitization is indeed caused by the Au_{25}-rod, we should observe upconverted fluorescence *via* triplet–triplet annihilation (TTA) between the ^{3}BPEA* (or ^{3}rubrene*) molecules (*i.e.*, delayed fluorescence). As shown in Fig. 3, when a deaerated mixture of the Au_{25}-rod and BPEA or rubrene was excited at 640 or 785 nm, respectively, upconverted fluorescence was clearly observed at wavelengths shorter than the excitation wavelength. Both fluorescences exhibited very long decays (in the order of 100 μs; see Fig. 3, insets). The time evolution of the UC intensity $I_{UC}(t)$, derived from the rate equation of the time dependence of the concentration of triplet emitter (^{3}E*) molecules considering the TTA process between ^{3}E*, is given by

$$I(t) = I(0)\left(\frac{1-\beta}{\exp(t/\tau_T)-\beta}\right)^2, \quad (1)$$

where τ_T is the lifetime of the ^{3}E* molecules and β is a dimensionless parameter between 0 and 1.[31] Eqn (1) accurately reproduces the observed decay profiles with τ_T = 127 μs and β = 0.25 for BPEA and τ_T = 104 μs and β = 0.18 for rubrene. These values are approximately four orders of magnitude longer than the fluorescence lifetimes of BPEA (3.3 ns in THF) and rubrene

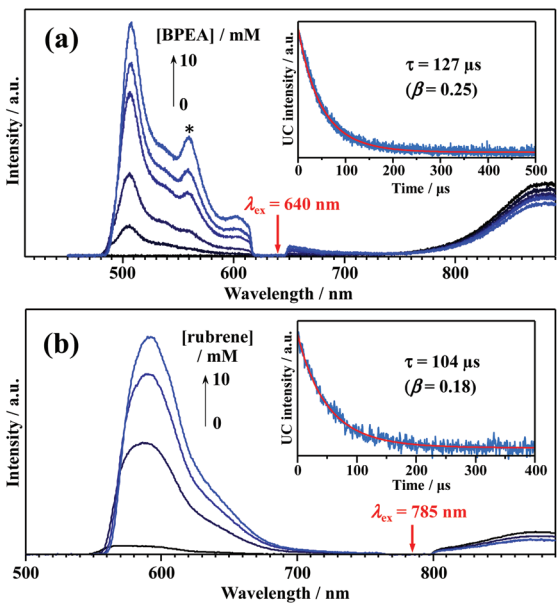

Fig. 3 PL emission spectra of (a) Au_{25}-rod (13 μM)/BPEA (0–10 mM) excited at 640 nm (10 W cm^{-2}) and (b) Au_{25}-rod (40 μM)/rubrene (0–10 mM) excited at 785 nm (5.5 W cm^{-2}) in deaerated THF. The asterisked peak in panel (a) begins to appear when the BPEA concentration exceeds ~5 mM and is assigned to the emission from BPEA aggregates (Fig. S4a†). Insets in panels (a and b) show the decay curves obtained by monitoring only the upconverted emission from BPEA and rubrene, respectively.

(10.8 ns in THF) shown in Fig. S7.† These facts confirm that the observed upconverted fluorescence is delayed fluorescence *via* the TTA between the BPEA (or rubrene) triplets sensitized by the Au_{25}-rod.

Recently, we proposed a relative method that estimates the Φ_{ISC} value of sensitizers by a TF-UC analysis.[29,32] The formation yield of the UC state (Φ_{UCs}), *i.e.*, the number of excited singlet states of the emitter ($^1E^*$) generated per number of photons absorbed by the sensitizer, can be experimentally evaluated as (see also Fig. S8†):[33]

$$\Phi_{UCs} = \frac{\Phi_{UC}}{\Phi_{out}(1-\Phi_q)\Phi_f}, \quad (2)$$

where Φ_{UC} is the uncorrected UC yield determined by the common relative method using an organic dye with a known fluorescence quantum yield (eqn (S1)). Φ_{out} represents the output coupling yield and corresponds to the correction for the loss of upconverted photons due to reabsorption by the sensitizer and emitter molecules. Φ_q is the quenching yield of $^3E^*$ by the sensitizer, and Φ_f is the fluorescence quantum yield of the emitter under UC measurement conditions (*i.e.*, at a very high emitter concentration). The Φ_{UCs} value is unique to the system and is determined by[33]

$$\Phi_{UCs} = \Phi_{ISC}\Phi_{TET}\Phi_{TTA}, \quad (3)$$

where Φ_{TET} and Φ_{TTA} represent the TET and TTA quantum yields, respectively. By definition, Φ_{TTA} is the product of the spin statistic factor η_c and the fraction of $^3E^*$ undergoing second-order decay f_2: explicitly, $\Phi_{TTA} = f_2 \cdot \eta_c/2$ (maximum value 0.5) where f_2 is given by[34]

$$f_2 = 1 - \frac{\beta - 1}{\beta}\ln(1-\beta). \quad (4)$$

The value of f_2 can be calculated from the β value of the UC decay fit using eqn (1). Finally, eqn (3) can be rewritten as

$$\Phi_{UCs} = \Phi_{ISC}\Phi_{TET}f_2\eta_c/2. \quad (5)$$

If the Φ_{UCs} value of the Au_{25}-rod/BPEA system is evaluated under the same experimental conditions (the same emitter concentration, solvent, and excitation source) as when evaluating Φ^r_{UCs} of the PdTPTBP (Φ_{ISC} = 0.97)[35]/BPEA reference system, the ratio Φ_{UCs}/Φ^r_{UCs} based on eqn (2) can be combined with eqn (5) to give the Φ_{ISC} value of the Au_{25}-rod. The formulation is as follows:

$$\Phi_{ISC} = \Phi^r_{ISC} \cdot \frac{\Phi^r_{TET}f^r_2}{\Phi_{TET}f_2} \cdot \frac{\Phi_{UC}/\Phi_{out}(1-\Phi_q)}{\Phi^r_{UC}/\Phi^r_{out}(1-\Phi^r_q)}. \quad (6)$$

In eqn (6), the superscript "r" refers to the reference system. Under the above-described experimental conditions, η_c can be regarded as identical in both systems and thereby cancels out. However, if the β values largely differ between the experimental and reference systems, the ratio f_2 must be retained in eqn (6). From the data and parameters shown in Fig. S9 and S10 and Tables S4–S6,† the Φ_{ISC} value of the Au_{25}-rod was determined as 0.99 ± 0.05. Thus, the phosphorescence quantum yield (Φ_p) was calculated as ~0.08 from the relation $\Phi_{PL} = \Phi_{ISC}\cdot\Phi_p$ (~0.08)[22] and the radiative rate constant (k_r) was calculated as 2.4×10^4 s^{-1} from the relation $\Phi_p\tau_{II}^{-1}$ (=$\Phi_p\tau_p^{-1}$, where τ_p represents the phosphorescence lifetime).

In a previous femtosecond TA spectroscopy study of the Au_{25}-rod,[16] excitation at 415 nm elicited sub-picosecond internal conversion (~0.8 ps) early time dynamics, but excitation at 775 nm yielded a constant feature of the TA spectra over a wide range of timescales (sub-ps to μs). In the present study, we showed that under excitation at 785 nm, the observed PL emission from the Au_{25}-rod is also phosphorescence (Fig. S2†); moreover, this coexistence with rubrene can induce the TF-UC phenomenon (Fig. 3b and Table S7†). Based on these experimental facts, we attributed the unchanged excited-state absorption signal to the T_1–T_n absorptions of the Au_{25}-rod, and the weak absorption shoulder at 730–900 nm mainly to the direct spin-forbidden transitions from S_0 to T_1 of the Au_{25}-rod, as shown in Fig. 4. The T_1–T_n absorption has been observed within a few picoseconds,[16] suggesting the occurrence of ultrafast ISC (~10^{12} s^{-1}). This inference is consistent with the almost 100% ISC efficiency and absence of fluorescence at room temperature. In time-dependent density functional theory calculations, the transitions between S_0 and S_1 were suggested to be symmetrically forbidden and their oscillator strength was zero (Fig. S11†).[22] In other words, the Au_{25}-rod cluster has the "dark" S_1 and "bright" T_1 states at room temperature.

In the biicosahedral Au_{25} core, the significant spin–orbit coupling effect provided by 25 Au atoms and the small S–T energy gap (<0.2 eV) is presumed to inevitably result in strong S–T mixing. Therefore, it may be more appropriate to view the excited states of such gold clusters as coherent superpositions of singlet and triplet states,[36] as in semiconductor nanocrystals with ill-defined spin quantum numbers.[37] If this is true, a clear distinction between fluorescence and phosphorescence

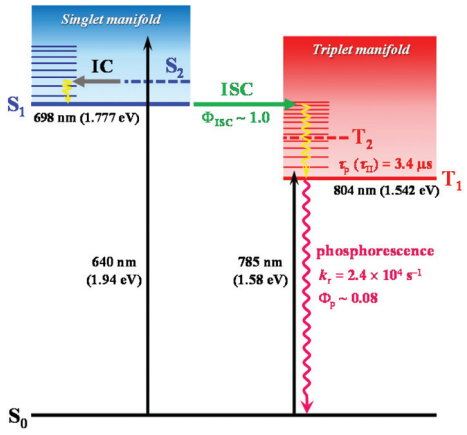

Fig. 4 Excited state deactivation pathway and related photophysical parameters for the Au_{25}-rod in deaerated THF. The vertical transition energy from S_0 to S_1 or T_1 obtained from theoretical calculations is also shown. The S_2 and T_2 states theoretically predicted to exist in the energetic vicinity of the S_1 and T_1 states (Fig. S11†) are shown as dashed lines.

would no longer be possible. Therefore, theoretical considerations based on total angular momenta (*i.e.*, the sum of orbital and spin angular momenta) may be necessary to better understand the electronic excited states and PL properties of noble metal clusters.

In conclusion, the observations and analysis of PL quenching and TF-UC of the biicosahedral Au_{25}-rod clusters confirmed that the PL from the Au_{25}-rod is phosphorescence from the excited triplet state formed with almost 100% ISC quantum yield. Moreover, this cluster behaves as a triplet sensitizer undergoing direct S–T transitions in the NIR region, which can induce NIR-to-visible photon upconversion. This gold superatomic molecule is capable of modifying its electronic states, photophysical properties, and hydrophobicity/hydrophilicity by altering thiolate ligands[15,23] or replacing the terminal Cl atoms with alkynyl ligands.[38] Hence, it is expected to be a nanomaterial with potential use as a triplet sensitizer in TF-UC applications.

Author contributions

MM conceptualized and designed the study, performed the computational work and wrote the manuscript. YW, RK, DA and YN performed experimental work and data analyses. All the authors discussed the results and contributed to the writing of the manuscript.

Conflicts of interest

There are no conflicts to declare.

Acknowledgements

This work is partly supported by the Grant-in-Aids for Young Scientists, no. 20K15110 and Scientific Research (C), no. 20K05653. Theoretical calculations were performed at the Research Center for Computational Science, Okazaki, Japan.

References

1 S. N. Khanna and P. Jena, *Phys. Rev. B: Condens. Matter Mater. Phys.*, 1995, **51**, 13705.
2 W. D. Knight, K. Clemenger, W. A. de Heer, W. A. Saunders, M. Y. Chou and M. L. Cohen, *Phys. Rev. Lett.*, 1984, **52**, 2141.
3 H. Häkkinen, *Chem. Soc. Rev.*, 2008, **37**, 1847.
4 Z. Luo and A. W. Castleman, Jr., *Acc. Chem. Res.*, 2014, **47**, 2931.
5 P. Jena and Q. Sun, *Chem. Rev.*, 2018, **118**, 5755.
6 S. Takano and T. Tsukuda, *J. Am. Chem. Soc.*, 2021, **143**, 1683.
7 H. Hirai, S. Ito, S. Takano, K. Koyasu and T. Tsukuda, *Chem. Sci.*, 2021, **11**, 12233.
8 Y. Shichibu, Y. Negishi, T. Watanabe, N. K. Chaki, H. Kawaguchi and T. Tsukuda, *J. Phys. Chem. C*, 2007, **111**, 7845.
9 K. Nobusada and T. Iwasa, *J. Phys. Chem. C*, 2007, **111**, 14279.
10 H. Qian, W. T. Eckenhoff, M. E. Bier, T. Pintauer and R. Jin, *Inorg. Chem.*, 2011, **50**, 10735.
11 J.-Q. Goh, S. Malola, H. Häkkinen and J. Akola, *J. Phys. Chem. C*, 2013, **117**, 22079.
12 M. Galchenko, R. Schuster, A. Black, M. Riedner and C. Klinke, *Nanoscale*, 2019, **11**, 1988.
13 G. Li and R. Jin, *J. Am. Chem. Soc.*, 2014, **136**, 11347.
14 S. Zhao, N. Austin, M. Li, Y. Song, S. D. House, J. C. Yang, G. Mpourmpakis and R. Jin, *ACS Catal.*, 2018, **8**, 4996.
15 K. Zheng, J. Zhang, D. Zhao, Y. Yang, Z. Li and G. Li, *Nano Res.*, 2019, **12**, 501.
16 M. Y. Sfeir, H. Qian, K. Nobusada and R. Jin, *J. Phys. Chem. C*, 2011, **115**, 6200.
17 M. S. Devadas, V. D. Thanthirige, S. Bairu, E. Sinn and G. Ramakrishna, *J. Phys. Chem. C*, 2013, **117**, 23155.
18 M. Zhou, J. Zhong, S. Wang, Q. Guo, M. Zhu, Y. Pei and A. Xia, *J. Phys. Chem. C*, 2015, **119**, 18790.
19 V. D. Thanthirige, E. Sinn, G. P. Wiederrecht and G. Ramakrishna, *J. Phys. Chem. C*, 2017, **121**, 3530.
20 S. Chen, H. Ma, J. W. Padelford, W. Qinchen, W. Yu, S. Wang, M. Zhu and G. Wang, *J. Am. Chem. Soc.*, 2019, **141**, 9603.
21 S. Park and D. Lee, *Langmuir*, 2012, **28**, 7049.
22 Q. Li, C. J. Zeman IV, Z. Ma, G. C. Schatz and X. W. Gu, *Small*, 2021, **17**, 2007992.
23 S. Wang, X. Meng, A. Das, T. Li, Y. Song, T. Cao, X. Zhu, M. Zhu and R. Jin, *Angew. Chem., Int. Ed.*, 2014, **53**, 2376.
24 K. Pyo, V. D. Thanthirige, K. Kwak, P. Pandurangan, G. Ramakrishna and D. Lee, *J. Am. Chem. Soc.*, 2015, **137**, 8244.
25 Y. Niihori, N. Takahashi and M. Mitsui, *J. Phys. Chem. C*, 2020, **124**, 5880.
26 T. N. Singh-Rachford and F. N. Castellano, *J. Phys. Chem. A*, 2008, **112**, 3550.
27 B. Valeur, *Molecular Fluorescence. Principles and Applications*, Wiley-VCH, 2001.
28 M. R. Padhye, S. P. McGlynn and M. Kasha, *J. Chem. Phys.*, 1956, **24**, 588.
29 Y. Niihori, Y. Wada and M. Mitsui, *Angew. Chem., Int. Ed.*, 2021, **60**, 2822.
30 F. M. Miranda, M. C. Menziani and A. Pedone, *J. Phys. Chem. C*, 2015, **119**, 10766.
31 E. M. Gholizadeh, L. Frazer, R. W. MacQueen, J. K. Gallahera and T. W. Schmidt, *Phys. Chem. Chem. Phys.*, 2018, **20**, 19500.
32 D. Arima, Y. Niihori and M. Mitsui, *J. Mater. Chem. C*, 2022, **10**, 4597.
33 Y. Zhou, F. N. Castellano, T. W. Schmidt and K. Hanson, *ACS Energy Lett.*, 2020, **5**, 2322.
34 Y. Y. Cheng, B. Fückel, T. Khoury, R. G. C. R. Clady, M. J. Y. Tayebjee, N. J. Ekins-Daukes, M. J. Crossley and

T. W. Schmidt, *J. Phys. Chem. Lett.*, 2010, **1**, 1795.
35 J. E. Rogers, K. A. Nguyen, D. C. Hufnagle, D. G. McLean, W. Su, K. M. Gossett, A. R. Burke, S. A. Vinogradov, R. Pachter and P. A. Fleitz, *J. Phys. Chem. A*, 2003, **107**, 11331.
36 Z. Wei, Y. Pan, X. Huo, Y. He, Y. Kuang, X. Ran and L. Guo, *J. Phys. Chem. C*, 2022, **126**, 3512.
37 Y. Han, S. He and K. Wu, *ACS Energy Lett.*, 2021, **6**, 3151.
38 M. Sugiuchi, Y. Shichibu, T. Nakanishi, Y. Hasegawa and K. Konishi, *Chem. Commun.*, 2015, **51**, 13519.